The Astrophysical Journal, 780:175 (10pp), 2014 January 10 doi:10.1088/0004-637X/780/2/175

OBLIQUE ALFVÉN INSTABILITIES DRIVEN BY COMPENSATED CURRENTS

P. Malovichko[1], Y. Voitenko[2], and J. De Keyser[2]
[1] Main Astronomical Observatory, NASU, Kyiv, Ukraine
[2] Solar-Terrestrial Centre of Excellence, Space Physics Division, Belgian Institute for Space Aeronomy, Ringlaan-3-Avenue Circulaire, B-1180 Brussels, Belgium; voitenko@oma.be
Received 2013 July 23; accepted 2013 November 16; published 2013 December 23

ABSTRACT

Compensated-current systems created by energetic ion beams are widespread in space and astrophysical plasmas. The well-known examples are foreshock regions in the solar wind and around supernova remnants. We found a new oblique Alfvénic instability driven by compensated currents flowing along the background magnetic field. Because of the vastly different electron and ion gyroradii, oblique Alfvénic perturbations react differently on the currents carried by the hot ion beams and the return electron currents. Ultimately, this difference leads to a non-resonant aperiodic instability at perpendicular wavelengths close to the beam ion gyroradius. The instability growth rate increases with increasing beam current and temperature. In the solar wind upstream of Earth's bow shock, the instability growth time can drop below 10 proton cyclotron periods. Our results suggest that this instability can contribute to the turbulence and ion acceleration in space and astrophysical foreshocks.

Key words: instabilities – ISM: supernova remnants – plasmas – solar wind – waves

Online-only material: color figures

1. INTRODUCTION

Current-driven instabilities are important for anomalous resistivity and related energy release in weakly collisional space plasmas like the solar corona, the solar wind, and planetary magnetospheres. Kinetic instabilities of ion-acoustic, ion-cyclotron, and lower-hybrid drift waves have been studied extensively in this context (Duijveman et al. 1981; Büchner & Elkina 2006 and references therein). More recently, electron-current driven kinetic Alfvén instabilities have been discussed as a possible source for the anomalous resistivity (Voitenko 1995) and the anomalous resistivity scaling in solar flares has been shown to be compatible with the kinetic Alfvén scenario (Singh & Subramanian 2007). These instabilities were classified as resonant instabilities driven by the inverse electron Landau damping (i.e., by the Cherenkov-resonant electrons). The off-resonant electrons with velocities far from the wave phase velocities interact with waves adiabatically and do not contribute to the wave growth.

On the contrary, the non-resonant current instability of the Alfvén mode (Malovichko & Iukhimuk 1992a, 1992b; Malovichko 2007) is driven by the total electric current rather than by the resonant electrons only. This "pure" current instability (PCI) was originally applied to the terrestrial auroral zones (Malovichko & Iukhimuk 1992a) and then studied in regards to the coronal loops in the solar atmosphere (Malovichko & Iukhimuk 1992b; Malovichko 2007; Chen & Wu 2012). PCI instabilities appeared to be universal in the sense that the threshold current is virtually zero in uniform unbounded plasmas.

Besides the applied external electric fields (electrostatic or inductive), electron and ion currents can also be induced in the background plasma by other sources such as injected particle beams. We are interested here in the cases where the currents injected by hot ion beams are compensated by the return currents of the background electrons (or by co-propagating electron beams). This situation occurs in many space and astrophysical plasmas. For example, high-energy ion beams accelerated by shocks set up compensated-current systems upstream of the terrestrial bow shock (Paschmann et al. 1981 and references therein) and around supernova remnants (Bell 2005 and references therein).

In addition to the current-driven instabilities discussed above, several ion-beam instabilities can develop in the compensated-current systems created by the ion beams. In the early works by Sentmann et al. (1981), Winske & Leroy (1984), and Gary (1985), it was believed that the parallel-propagating Alfvén and fast modes are most unstable. Later on, the resonant oblique (kinetic) Alfvén instabilities driven by ion beams were shown to be more important in certain parameter ranges. So, analytical treatments (Voitenko 1998; Voitenko & Goossens 2003; Verscharen & Chandran 2013) and numerical simulations (Daughton et al. 1999; Gary et al. 2000) have demonstrated that the ion-cyclotron (Alfvén I in the terminology of Daughton et al.) and Cherenkov (Alfvén II) instabilities of oblique Alfvén waves are often faster than the parallel ones. These instabilities were in particular studied in application to the α-particle flows in the solar wind (Gary et al. 2000; Verscharen & Chandran 2013).

Because of the incomplete knowledge of plasma instabilities that can arise, the behavior of such complex systems is still not well understood. For example, the evolution of the ions reflected from the terrestrial bow shock and responsible waves and instabilities remain uncertain. The same concerns cosmic ray acceleration by the shocks around supernova remnants. It is important to know what instabilities can arise there and which one dominates for particular beam and plasma parameters. Recently, a new magnetohydrodynamic (MHD)-type instability driven by the return currents induced by cosmic rays in the foreshock plasma around supernova remnants was found by Bell (2004, 2005). A similar return-current instability was found earlier by Winske & Leroy (1984), but they did not elucidate the main physical factor leading to the instability and hence did not categorize it as current-driven.

In the present paper, we investigate a new non-resonant instability that arises in the compensated-current systems created by fast and hot ion beams. In such systems, the beam current is compensated by the return background current and one should

not expect the PCI studied by Malovichko & Iukhimuk and by Chen & Wu. However, oblique Alfvén perturbations with short perpendicular wavelengths respond differently to the currents carried by the electrons and the currents carried by the ions. The difference arises because of the different ion and electron gyroradii, such that the ion and electron-current-related terms do not cancel each other. The resulting compensated-current oblique instability (CCOI) develops at sufficiently high beam currents and temperatures. The instability is essentially oblique and its growth rate attains a maximum when its cross-field wavelength is close to the beam ion gyroradius.

2. PROBLEM SETUP

A particular compensated-current system is considered consisting of the low-density hot ion beam propagating along $\mathbf{B}_0$, the motionless background ions, and the electron components providing the neutralizing return current. The neutralizing electron current can be set up by the background electron component and/or by the co-propagating electron beam. In the context of our study, it is important to note that the final result does not depend on how the return electron current is set up; it is enough that the gyroradius of the current-carrying electrons is much smaller than the ion-beam gyroradius.

For each unperturbed plasma component, we use a u_α-shifted Maxwellian velocity distribution

$$f_{0\alpha} = \frac{n_\alpha}{(2\pi T_\alpha/m_\alpha)^{3/2}} \exp\left(-\frac{m_\alpha v_\perp^2}{2T_\alpha} - \frac{m_\alpha (v_z - u_\alpha)^2}{2T_\alpha}\right), \quad (1)$$

where n_α, T_α, and u_α are the mean number density, temperature, and parallel velocity, respectively, and m_α is the particle mass. The species α can be background ions (i), background electrons (e), beam ions (b), and beam electrons (be). The subscripts z and $\perp$ indicate directions parallel and perpendicular to the mean magnetic field $\mathbf{B}_0$.

The plasma is assumed to be charge-neutral $\sum_\alpha q_\alpha n_\alpha = 0$ and current-neutral, $\sum_\alpha q_\alpha n_\alpha u_\alpha = 0$. In the reference system of background protons, the zero net current condition reads as

$$\sum_e n_e u_{ze} = n_b u_b, \quad (2)$$

where the summation is over all of the electron components.

To study electromagnetic perturbations in such a system, we use a kinetic plasma model, where the velocity distribution function of each species α obeys the collisionless Vlasov equation

$$\frac{\partial f_\alpha}{\partial t} + \mathbf{v}\frac{\partial f_\alpha}{\partial \mathbf{r}} + \frac{q_\alpha}{m_\alpha}\left(\mathbf{E} + \frac{1}{c}[\mathbf{v}\times\mathbf{B}]\right)\frac{\partial f_\alpha}{\partial \mathbf{v}} = 0. \quad (3)$$

The self-consistent electric $\mathbf{E}$ and magnetic $\mathbf{B}$ fields obey Maxwells equations with the charge density $\sum_\alpha q_\alpha \int d^3v f_\alpha$ and the current density $\sum_\alpha q_\alpha \int d^3v \mathbf{v} f_\alpha$, q_α and m_α are the particles charge and mass, respectively, t is time, $\mathbf{r}$ represents spatial coordinates, and $\mathbf{v}$ represents velocity-space coordinates.

3. LOW-FREQUENCY ALFVÉNIC SOLUTION

Linearizing (3) and Maxwells equations around unperturbed state ($f_\alpha = f_{0\alpha} + \delta f$, $\mathbf{E} = \mathbf{E}_0 + \delta\mathbf{E}$, $\mathbf{B} = \mathbf{B}_0 + \delta\mathbf{B}$), one can reduce the resulting linear Vlasov–Maxwell set of equations to three equations for three components of the perturbed electric field δE_x, δE_y, and δE_z. The nontrivial solutions to the Maxwell–Vlasov set of equations, $\delta\mathbf{E} \neq 0$, exist if the wave frequency ω and the wavevector $\mathbf{k} = (k_x, 0, k_z)$ satisfy the following dispersion equation (e.g., Alexandrov et al. 1984):

$$\left| k^2\delta_{ij} - k_i k_j - \frac{\omega^2}{c^2}\varepsilon_{ij} \right| = 0, \quad (4)$$

where ε_{ij} is the dielectric tensor and δ_{ij} is the Kronecker delta symbol. Using expressions for the elements ε_{ij} given by Alexandrov et al. (1984), we reduced them in the low-frequency domain ($(\omega'/\omega_{Bi})^2 \ll 1$ and $(k_z V_{T\alpha}/\omega_{B\alpha})^2 \ll 1$) as follows:

$$\begin{aligned}
\varepsilon_{xx} &\simeq 1 + \sum_\alpha \left(\frac{\omega_{P\alpha}}{\omega_{B\alpha}}\right)^2 \left(\frac{\omega'_\alpha}{\omega}\right)^2 \frac{\left(1 - A_0\left(\mu_\alpha^2\right)\right)}{\mu_\alpha^2}, \\
\varepsilon_{xy} &= -\varepsilon_{yx} \simeq -i\sum_\alpha \left(\frac{\omega_{P\alpha}^2}{\omega_{B\alpha}}\right)\left(\frac{\omega'_\alpha}{\omega^2}\right) A'_0\left(\mu_\alpha^2\right), \\
\varepsilon_{xz} &= \varepsilon_{zx} \simeq \sum_\alpha \left(\frac{\omega_{P\alpha}}{\omega_{B\alpha}}\right)^2 \left(\frac{\omega'_\alpha k_x u_\alpha}{\omega^2}\right) \frac{\left(1 - A_0\left(\mu_\alpha^2\right)\right)}{\mu_\alpha^2}, \\
\varepsilon_{yy} &\simeq \varepsilon_{xx} + 2\sum_\alpha \left(\frac{\omega_{P\alpha}}{\omega}\right)^2 \mu_\alpha^2 A'_0(\mu_\alpha^2) J_+(\xi_\alpha), \\
\varepsilon_{yz} &= -\varepsilon_{zy} \simeq -i\frac{k_x}{k_z}\sum_\alpha \left(\frac{\omega_{P\alpha}^2}{\omega_{B\alpha}\omega}\right) A'_0\left(\mu_\alpha^2\right)\left[1 - J_+(\xi_\alpha)\right], \\
\varepsilon_{zz} &\simeq 1 + \sum_\alpha \left(\frac{\omega_{P\alpha}}{k_z V_{T\alpha}}\right)^2 A_0\left(\mu_\alpha^2\right)\left[1 - J_+(\xi_\alpha)\right] \\
&\quad + \sum_\alpha \left(\frac{\omega_{P\alpha}}{\omega_{B\alpha}}\right)^2 \left(\frac{k_x u_\alpha}{\omega}\right)^2 \frac{\left(1 - A_0\left(\mu_\alpha^2\right)\right)}{\mu_\alpha^2},
\end{aligned} \quad (5)$$

where $\omega'_\alpha = \omega - k_z u_\alpha$, $A_0(\mu_\alpha^2) = I_0(\mu_\alpha^2)\exp(-\mu_\alpha^2)$, $I_0(\mu_\alpha^2)$ is the zero-order modified Bessel function, $\mu_\alpha = k_x V_{T\alpha}/\omega_{B\alpha}$ is the normalized perpendicular wavenumber, $A'_0(x) = dA_0(x)/dx$, $\omega_{P\alpha}$ ($\omega_{B\alpha}$) is the plasma (cyclotron) frequency, $V_{T\alpha} = \sqrt{T_\alpha/m_\alpha}$ is the thermal velocity, and $\xi_\alpha = \omega'_\alpha/(k_z V_{T\alpha})$.

We found that the function $J_+(\xi_\alpha)$ (Alexandrov et al. 1984),

$$J_+(\xi_\alpha) = \xi_\alpha \exp\left(-\frac{\xi_\alpha^2}{2}\right)\int_{i\infty}^{\xi_\alpha} dt \exp\left(\frac{t^2}{2}\right), \quad (6)$$

is particularly useful in the context of the present study. This function is related to the well-known plasma W-function, $J_+(x) = -i\sqrt{\pi/2}\,x\,W(x/\sqrt{2})$, and can be expanded in the small- and large-argument series:

$$J_+(x) = x^2 + O\left(x^4\right) - i\sqrt{\frac{\pi}{2}}\,x\exp\left(-\frac{x^2}{2}\right), \quad |x| \ll 1, \quad (7)$$

and

$$J_+(x) = 1 + \frac{1}{x^2} + O\left(\frac{1}{x^4}\right) - i\eta\sqrt{\frac{\pi}{2}}\,x\exp\left(-\frac{x^2}{2}\right), \quad |x| \gg 1, \quad (8)$$

where $\eta = 0$ for $\mathrm{Im}x > 0$, $\eta = 1$ for $\mathrm{Im}x = 0$, and $\eta = 2$ for $\mathrm{Im}x < 0$.

In low-β plasmas, where the gas/magnetic pressure ratio of the background plasma $\beta < 1$, and for perpendicular wavelengths smaller than the background ion gyroradius,

$\mu_i^2 \ll 1$, the dispersion equation (Equation (4)) reduces to

$$\left(\omega^2 - k_z^2 V_A^2\right)\left(\omega^2 - k^2 V_A^2\right) \simeq \omega_{Bi}^2 k_z^2 V_A^2 \left(1 + A_0'(\mu_b^2)\right)^2 \bar{j}_b^2, \tag{9}$$

where $V_A = B_0/\sqrt{4\pi n_i m_i}$ is the background Alfvén velocity, n_i is the background ion number density, $\bar{j}_b = n_b V_b / n_i V_A$ is the ion-beam current $j_b = e n_b V_b$ normalized by the Alfvén current $j_A = e n_i V_A$, and V_b is the mean beam velocity (e is the proton charge and we assumed that the ions are protons). When deriving Equation (9), we used the expansion (7) for the background electron $J_+(\xi_e)$, the expansion (8) for the background ion $J_+(\xi_i)$, the zero net current condition (2), and we dropped small beam terms containing the functions $J_+(\xi_b)$ and $J_+(\xi_{be})$. The expansion (8) is already good for $J_+(\xi_i)$ at $\xi_i \gtrsim 2$, where the relative error is less than 0.1. Note that $\mu_i^2 \ll 1$ does not imply $\mu_b^2 = (T_b/T_i)\mu_i^2 \ll 1$ if the beam is hotter than the background.

In the absence of compensated currents, $\bar{j}_b = j_e = 0$, Equation (9) splits into two independent equations for MHD Alfvén and fast mode waves (the slow mode was dropped from Equation (9) because of the low plasma β). In the presence of $\bar{j}_b$, the Alfvén and fast mode waves are coupled and the solution corresponding to Alfvén mode reads as

$$\omega^2 = k_z^2 V_A^2 + \frac{1}{2}\left(k_x^2 V_A^2 - \sqrt{k_x^4 V_A^4 + 4\omega_{Bi}^2 k_z^2 V_A^2 \left(1 + A_0'(\mu_b^2)\right)^2 \bar{j}_b^2}\right). \tag{10}$$

The dispersion relation (Equation (10)) for Alfvénic perturbations provides a basis for our analysis. The current term containing $\bar{j}_b$ shifts down the Alfvén wave frequency squared and can make it negative, which means an aperiodic instability. The fast mode solution is up-shifted and remains stable; we will not consider it here.

4. INSTABILITY ANALYSIS

4.1. Threshold

It is easy to see from Equation (10) that the frequency becomes purely imaginary, $\omega^2 < 0$, when the beam current is sufficiently high:

$$\bar{j}_b > \frac{\mu_b}{\left(1 + A_0'(\mu_b^2)\right)}\left(\frac{k}{k_x}\right)\left(\frac{V_A}{V_{Tb}}\right). \tag{11}$$

The function $\mu_b/(1 + A_0'(\mu_b^2)) \to \infty$ in the limits $\mu_b \to 0$ and $\mu_b \to \infty$ attains a minimum $\simeq 1.33$ at $\mu_b \simeq 0.89$. This minimum defines the instability threshold current

$$\bar{j}_{\rm thr} \simeq 1.33 \frac{V_A}{V_{Tb}}. \tag{12}$$

Formally, the instability threshold is achieved at $k_z = 0$. However, in reality, k_z has a lower bound defined by the parallel system scale, $k_z \gtrsim 2\pi/L_z$. This limitation does not alter the above threshold estimation for realistic system length scales larger than the beam ion gyroradius, $L_z \gg \rho_b$, $\rho_b = V_{Tb}/\omega_{Bi}$.

As an example, we compare the threshold of the CCOI (Equation (12)) in the form

$$\left(\frac{n_b}{n_i}\right)_{\rm min}\left(\frac{V_b}{V_A}\right) > 1.33\left(\frac{V_A}{V_{Tb}}\right), \tag{13}$$

with the threshold of the fire-hose instability (FHI) in streaming plasmas (e.g., Voitenko et al. 1980):

$$\left(\frac{n_b}{n_i}\right)_{\rm min}\left(\frac{V_b}{V_A}\right)^2 > 1 + \Delta, \tag{14}$$

where anisotropy effects represented by Δ include plasma β (temperature) anisotropies and heat flux (q) anisotropies:

$$\Delta = \sum_{s=i,b}\left(\frac{\beta_{s\perp} - \beta_{s\parallel}}{2}\right) + \frac{8\pi k}{\omega_{Bi} B_0^2}\sum_{s=i,b}(q_{s\perp} - q_{s\parallel}).$$

Both $\Delta > 0$ and $\Delta < 0$ cases occur in the solar wind with $\Delta > 0$ dominated by anisotropic ion cores and $\Delta < 0$ dominated by parallel electron strahls and halos and by parallel ion tails and beams (Marsch 2006 and references therein). In general, the beam-driven fire-hose threshold is reduced by $\Delta < 0$ and increased by $\Delta > 0$. We will consider hereafter only the isotropic case $\Delta = 0$, implying a pure beam-driven FHI.

A comparison of the CCOI and FHI thresholds is shown in Figure 1 for the case of the hot beam, $V_{Tb}/V_A = 20$, in the isotropic background, $\Delta = 0$. The CCOI threshold for such a hot beam is significantly lower than the FHI threshold for a wide range of beam velocities. These parameter ranges are relevant for compensated-current systems created in the solar wind by hot ion beams propagating upstream of the terrestrial bow shock (additional details are given below).

The parallel-propagating, left- and right-handed resonant instabilities studied by Gary (1985) have velocity thresholds $V_{b\rm thr}^-/V_A \sim 0.82$ and $V_{b\rm thr}^+/V_A \sim 1$, respectively. The CCOI velocity threshold found from Equation (13),

$$\frac{V_{b\rm thr}^{\rm CCOI}}{V_A} = 1.33\left(\frac{n_i V_A}{n_b V_{Tb}}\right),$$

is lower than both thresholds of resonant instabilities $V_{b\rm thr}^{\pm}/V_A$ provided that

$$\frac{V_{Tb}}{V_A} > 1.6\frac{n_i}{n_b}.$$

This condition is not easily satisfied in terrestrial foreshocks. Say, for a relatively high-density beam, $n_b/n_i \simeq 0.1$, it is satisfied if the beam is also quite hot $V_{Tb}/V_A \geqslant 16$. However, as is shown below, the CCOI can be the strongest instability in the parameter range where several instabilities are over the threshold.

4.2. Wavenumber Dependence of the Instability Increment

To analyze the CCOI growth rate $\gamma = {\rm Im}(\omega)$ as a function of wavevector components, we rewrite Equation (10) in the dimensionless form:

$$\frac{\gamma}{\omega_{Bi}} = \sqrt{\sqrt{0.25\left(\frac{V_A}{V_{Tb}}\right)^4 \mu_b^4 + \bar{j}_b^2\left(1 + A_0'(\mu_b^2)\right)^2\left(\frac{k_z V_A}{\omega_{Bi}}\right)^2} - \left(\frac{k_z V_A}{\omega_{Bi}}\right)^2 - 0.5\mu_b^2\left(\frac{V_A}{V_{Tb}}\right)^2}. \tag{15}$$

We choose the normalization for the perpendicular wavenumber $\mu_b = k_\perp \rho_b$, which simplifies the analysis of the current term containing $A_0'(\mu_b^2)$.

The full wavenumber dependence of the CCOI dispersion (Equation (15)) is shown in the contour plot in Figure 2 for the beam current $\bar{j}_b = 0.3$ that is well above the threshold and the thermal velocity $V_{Tb}/V_A = 20$. It is seen that the instability increment has a well-defined maximum in the $(k_z, k_\perp)$ plane. The instability boundary in the $(k_z, k_\perp)$ plane is shown in Figure 2 by the outer dashed line. All wavenumbers inside the area below this line are unstable. It is seen that the instability range is bounded in $k_\perp$-space and both the lower and upper bounds, μ_{b1} and μ_{b2}, are finite and non-zero. In contrast, the lower bound of the unstable parallel wavenumber range is zero. For currents that are well over the threshold, the analytical

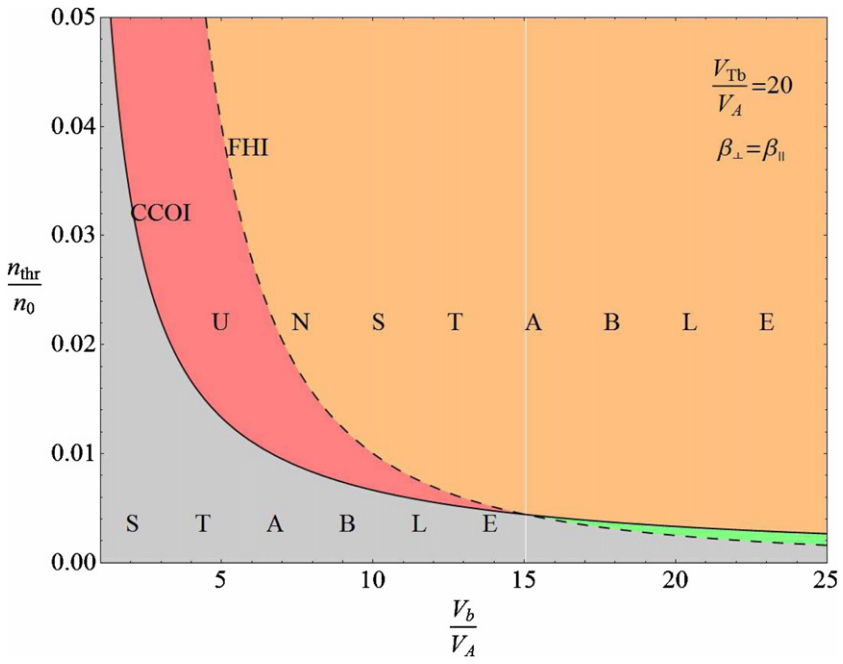

Figure 1. Comparison of the thresholds for the FHI and CCOI. The beam thermal velocity is $V_{Tb}/V_A = 20$ and the plasma temperature is isotropic. The CCOI threshold is lower in the wide range of beam velocities $V_b/V_A < 15$.

(A color version of this figure is available in the online journal.)

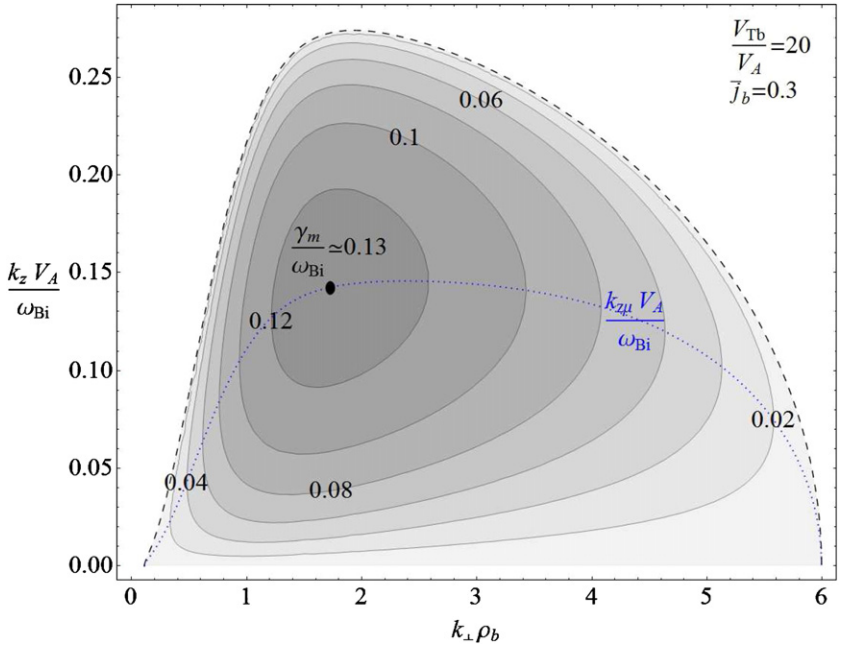

Figure 2. Contours of the CCOI growth rate as a function of the normalized parallel and perpendicular wavenumbers. The normalized beam current is $\bar{j}_b = 0.3$ and thermal velocity is $V_{Tb}/V_A = 20$. The absolute maximum of the CCOI, $\gamma_{\rm m}/\omega_{Bi} \simeq 0.13$, is shown by the black dot. The instability threshold (dashed outer contour) encircles the range of unstable wavenumbers. The parallel wavenumber $k_{z\mu}V_A/\omega_{Bi}$, corresponding to the local maximum γ_μ/ω_{Bi}, is shown by the blue dotted line.

(A color version of this figure is available in the online journal.)

expressions for the boundaries in k-space can be written as

$$\mu_{b2} \simeq \bar{j}_b \frac{V_{Tb}}{V_A}\frac{k_x}{k}$$

for the high $k_\perp$ boundary and

$$\mu_{b1} \simeq \frac{2}{3\mu_{b2}}$$

for the low $k_\perp$ boundary.

Since the lower bound of unstable k_z is zero, very long parallel wave lengths can be generated by the CCOI. However, there are several limitations on small k_z imposed by the finite field-aligned dimension of the system and/or the timescale of the system variability. The latter limitation is related to the fact that the instability growth time increases with decreasing k_z and at some finite k_z becomes longer than the characteristic evolution time of the system.

The k_z dependence of the CCOI dispersion is shown for several values of $\bar{j}_b$ in Figure 3. For each $\bar{j}_b$, we fix $k_\perp$

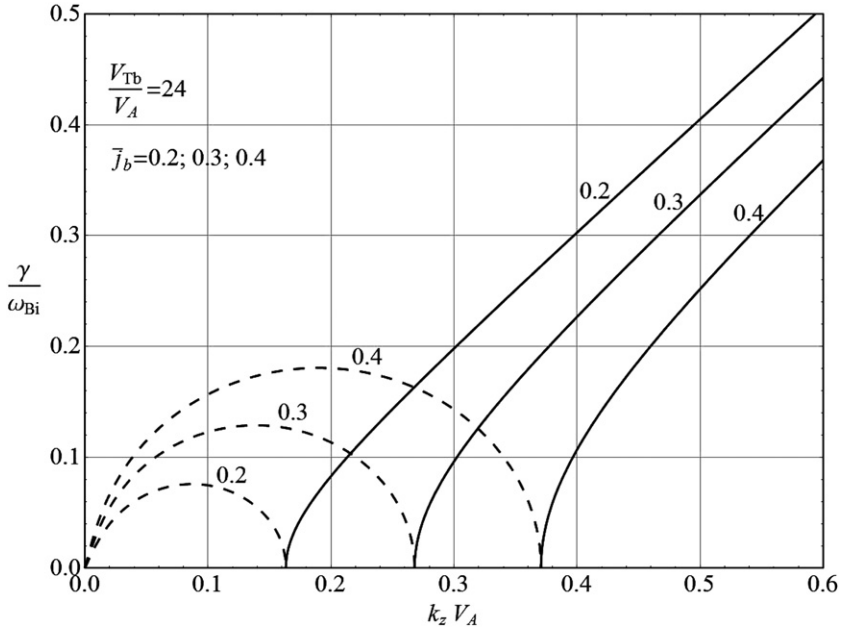

Figure 3. The CCOI growth rate (dashed lines) as a function of the normalized parallel wavenumber $k_z V_A/\omega_{Bi}$ for different beam currents $\bar{j}_b = 0.2$, 0.3, and 0.4 (for the lines from bottom to top). The waves are aperiodically unstable at small $k_z V_A/\omega_{Bi}$ and then become current-modified Alfvén waves at larger $k_z V_A/\omega_{Bi}$ with real frequencies (solid lines).

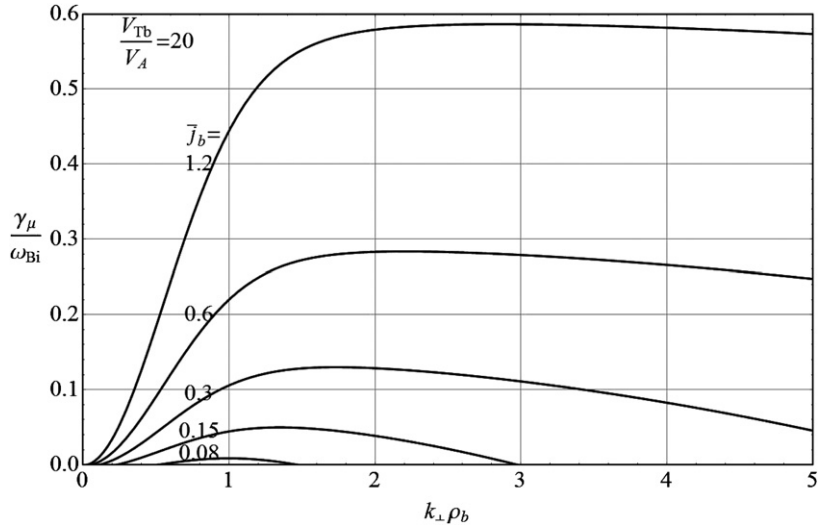

Figure 4. The CCOI growth rate at the local maximum γ_μ/ω_{Bi} as a function of the normalized perpendicular wavenumber $k_\perp \rho_b$ for different beam currents $\bar{j}_b = 1.2$, 0.6, 0.3, 0.15, and 0.08 (for the lines from top to bottom). The range of unstable wavenumbers extends with growing $\bar{j}_b$.

at the value where the CCOI increment $\gamma = \mathrm{Im}(\omega)$ passes through the absolute maximum. At small k_z, there is an unstable wavenumber range where the mode is aperiodically growing. The increment first increases linearly with k_z, then its increase slows down and attains a maximum and then it decreases to zero. At larger k_z, above this zeropoint, the CCOI dispersion becomes real and describes the usual Alfvén wave with a frequency shifted down by the compensated-current effects (shown by the solid line in Figure 3).

The easiest way to find the absolute maximum of Equation (15) is first to find a local maximum of γ with respect to k_z. This can be done analytically and for arbitrary μ_b we find

$$\frac{\gamma_\mu}{\omega_{Bi}} = \frac{1}{2}\left(\bar{j}_b\left(1 + A_0'\left(\mu_b^2\right)\right) - \left(\frac{V_A}{V_{Tb}}\right)^2 \frac{\mu_b^2}{\bar{j}_b\left(1 + A_0'\left(\mu_b^2\right)\right)}\right). \tag{16}$$

This maximum is attained at

$$\frac{k_{z\mu} V_A}{\omega_{Bi}} = \frac{1}{2}\sqrt{\bar{j}_b^2\left(1 + A_0'\left(\mu_b^2\right)\right)^2 - \left(\frac{V_A}{V_{Tb}}\right)^4 \frac{\mu_b^4}{\bar{j}_b^2\left(1 + A_0'\left(\mu_b^2\right)\right)^2}}. \tag{17}$$

The perpendicular wavenumber dependence of the increment γ_μ is shown in Figure 4 for $V_{Tb}/V_A = 20$ and for several values of the beam current $\bar{j}_b = 0.08$ (the near-threshold value), 0.15, 0.3, 0.6, and 1.2. We see that with growing $\bar{j}_b$, the perpendicular wavenumber $\mu_{b\mathrm{m}}$, at which the instability increment attains the absolute maximum γ_m, increases. Also, the range of unstable μ_b widens, such that smaller and larger perpendicular wavenumbers are excited. This especially concerns higher $\mu_b > \mu_{b\mathrm{m}}$, where the increment is decreasing slowly and remains large, comparable with the maximum value γ_m. On the other hand,

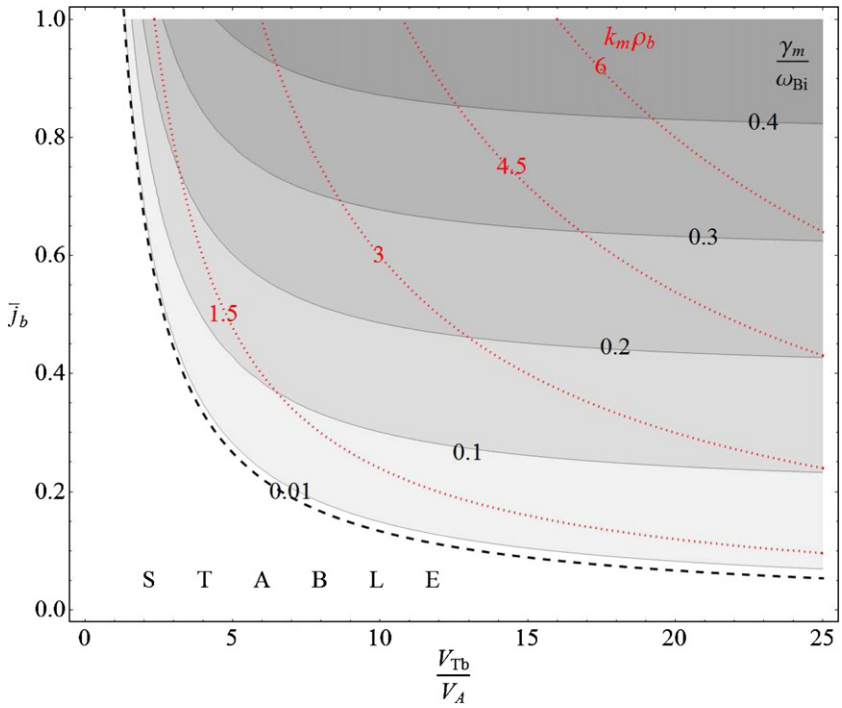

Figure 5. Contour plot of the maximum CCOI growth rate γ_m/ω_{Bi} (solid lines and shading) as a function of the beam current and thermal velocity. At large beam thermal velocities $V_{Tb}/V_A > 15$, the CCOI growth rate is almost independent of V_{Tb}/V_A (the asymptotic instability regime). The contours of the corresponding perpendicular wavenumber $k_{m\perp}\rho_b$ (dotted red lines) are superimposed. Larger $k_{m\perp}$ are generated at larger beam currents and temperatures. The instability boundary is shown by the dashed line.

(A color version of this figure is available in the online journal.)

in this high-μ_b range, the finite gyroradius effects may become important not only for the beam, but also for the background protons. The finite μ_i corrections that are neglected here will be investigated in our forthcoming study.

The μ_b dependence of $k_{z\mu}$ (Equation (17)) is shown in Figure 2 by the blue dotted line. At certain points along this line, $\mu_b = \mu_{bm}$ and $k_z = k_{zm}$, the increment attains the absolute maximum $\gamma_\mu = \gamma_m$ for the given plasma parameters. The absolute maximum defines the instability growth rate. In general, the normalized wavenumbers at maximum, μ_{bm} and $k_{zm}V_A/\omega_{Bi}$, depend on the beam current $\bar{j}_b$ and thermal velocity V_{Tb}/V_A. In Figure 2, where $\bar{j}_b = 0.3$ and $V_{Tb}/V_A = 20$, the maximum $\gamma_m \simeq 0.13\omega_{Bi}$ is achieved with $\mu_{bm} \simeq 1.73$ and $k_{zm}V_A/\omega_{Bi} \simeq 0.14$. The same values can also be fond in Figure 4 at the maximum of the curve for $\bar{j}_b = 0.3$.

4.3. Asymptotic Scalings

From Equation (16), it is possible to obtain two important scaling relations for the instability growth rate γ_m. In the "near-threshold" regime, where $\bar{j}_b < 3\bar{j}_{thr}$, the instability growth rate γ_m is proportional to the excess of the beam current over the threshold one:

$$\gamma_m \simeq 0.67(\bar{j}_b - \bar{j}_{thr})\omega_{Bi}. \quad (18)$$

This maximum is achieved at $\mu_{bm} \simeq 0.9$ and

$$\frac{k_{zm}V_A}{\omega_{Bi}} \simeq 0.34\sqrt{\bar{j}_b^2 - \frac{\bar{j}_{thr}^4}{\bar{j}_b^2}}.$$

Well above the threshold, $\bar{j}_b > 3\bar{j}_{thr}$, the maximum growth rate has the following linear scaling with the beam current to the leading order:

$$\gamma_m \simeq 0.5\bar{j}_b\omega_{Bi}. \quad (19)$$

In this well-over-threshold regime, the dependence of μ_{bm} on the beam and plasma parameters can be approximated analytically by the following expression:

$$\mu_{bm} \simeq 0.8\left(\frac{V_{Tb}}{V_A}\bar{j}_b\right)^{2/5}. \quad (20)$$

The approximate small-$\bar{j}_b$ and large-$\bar{j}_b$ expressions (Equations (18) and (19)) connect smoothly in the intermediate range of currents $\bar{j}_b \sim 3\bar{j}_{thr}$, which means they can be used for the growth-rate estimations at all currents.

4.4. Growth Rate and Inclination Angle of the CCOI

The CCOI growth rate is determined by the absolute maximum of the instability increment in the wavenumber space γ_m. We also define the instability wavenumber as the wavenumber $\mathbf{k}_m = (k_{\perp m}, 0, k_{zm})$ where the instability increment attains the absolute maximum γ_m.

The contour plot of the CCOI growth rate γ_m is shown in Figure 5 as a function of $\bar{j}_b$ (the beam current is in units of the Alfvén current) and V_{Tb}/V_A (the beam thermal velocity is in units of the Alfvén velocity). Contours for γ_m are solid and emphasized by the shadowing, such that the darker areas are more unstable. The full normalized wavenumber $k_m\rho_b$ of the most unstable perturbations generated by the CCOI is shown by dotted contours. In general, the instability is stronger and generates larger wavenumbers at larger beam currents and larger thermal velocities.

The instability threshold in the $(\bar{j}_b, V_{Tb})$ plane is shown by the dashed line, such that the range of beam currents and thermal velocities above this line is CCOI-unstable. The threshold is very close to the outer contour $\gamma_m/\omega_{Bi} = 0.01$. It is seen

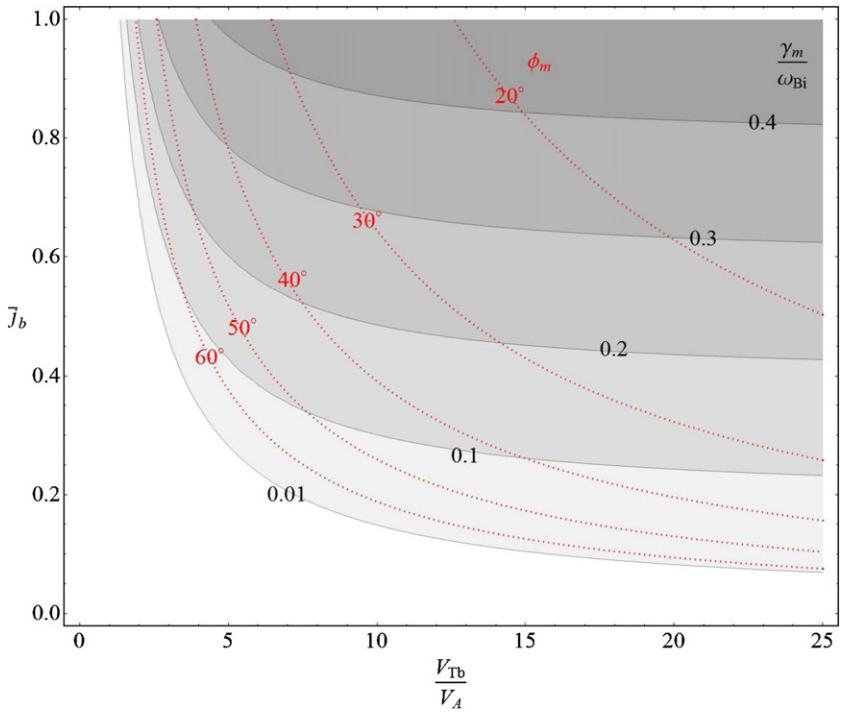

Figure 6. Same as in Figure 5, but with a wavevector tilt angle ϕ_m (red dotted lines; values are in degrees) superimposed on the CCOI growth rate γ_m/ω_{Bi} (gray solid lines with shading). Less oblique waves are generated by hotter beams.

(A color version of this figure is available in the online journal.)

from Figure 5 that the increasing beam temperature favors the instability, making the CCOI growth rate larger and the threshold current lower. In the wide range of beam thermal velocities, $5 < V_{Tb}/V_A < 25$, the instability is quite strong, $\gamma_m \simeq (0.1\text{–}0.2)\omega_{Bi}$, with moderate beam currents $j_b \sim 0.4$.

It is interesting to estimate ϕ_m, the wavevector tilt angle of most unstable perturbations with respect to the mean magnetic field. This angle is given by

$$\mathrm{tg}\,(\phi_m) = \frac{k_{\perp m}}{k_{zm}} = \frac{\mu_{bm}}{k_{zm}V_A/\omega_{Bi}}\frac{V_A}{V_{Tb}}. \qquad (21)$$

In the case described above of $\bar{j}_b = 0.3$ and $V_{Tb}/V_A = 20$, it is $\phi_m \simeq 32^\circ$. The tilt angle ϕ_m as a function of $\bar{j}_b$ and V_{Tb}/V_A is shown in Figure 6. From this figure, one can see that only oblique fluctuations are generated by the CCOI. In the near-threshold regime, the generated perturbations are very oblique, $45^\circ < \phi_m < 90^\circ$. However, with growing $\bar{j}_b$ and/or V_{Tb}/V_A, the wavevector tilt angle quickly decreases and in the well-over-threshold regime the tilt angles are relatively small, $\phi_m \lesssim 20^\circ$.

In the near-threshold and well-over-threshold regimes, the tilt angle can be estimated from the following scaling relations:

$$\begin{cases} \mathrm{ctg}\,(\phi_m) \simeq 0.38\sqrt{\bar{j}_b^2 - \bar{j}_{\mathrm{thr}}^2\left(\frac{\bar{j}_{\mathrm{thr}}}{\bar{j}_b}\right)^2} & \text{for} \quad \bar{j}_{\mathrm{thr}} < \bar{j}_b < 2\bar{j}_{\mathrm{thr}}, \\ \mathrm{ctg}\,(\phi_m) \simeq 0.76\left(\frac{\bar{j}_b}{\bar{j}_{\mathrm{thr}}}\right)^{3/5} & \text{for} \quad 3\bar{j}_{\mathrm{thr}} \leqslant \bar{j}_b < 2. \end{cases} \qquad (22)$$

5. CCOI INSTABILITIES IN THE SOLAR WIND UPSTREAM OF THE TERRESTRIAL BOW SHOCK

As a possible example where the CCOI can develop, we consider compensated-current systems created by proton beams propagating upstream of the terrestrial bow shock. The observed proton beams can be categorized into three classes (Paschmann et al. 1981; Tsurutani & Rodriguez 1981): (1) fast beams with temperatures $10^6 < T_b < 10^7$ K and velocities (in the solar-wind frame) $10 < V_b/V_A < 25$ created by the protons "reflected" from the quasi-perpendicular shocks, (2) slow hot beams with $5{\cdot}10^7 < T_b \lesssim 10^8$ K and $1 < V_b/V_A < 7$ created by "diffuse" protons upstream of the quasi-parallel shocks, and (3) "intermediate" beams with $T_b \gtrsim 10^7$ K and $V_b/V_A \sim 10$ observed in the regions in between. The beam number densities are similar for all three classes and vary in the range $n_b/n_0 = 0.01\text{–}0.1$.

1. The "reflected" beams propagate from quasi-perpendicular shocks with high velocities $V_b/V_A = 15$ (which, with $n_b/n_0 = 0.03$, gives $\bar{j}_b = 0.45$) and $V_{Tb}/V_A = 5$. With these "representative" values, we estimate the growth rate $\gamma_m/\omega_{Bi} \simeq 0.08$ attained at $\mu_{bm} = 1.1$, $k_{zm}V_A/\omega_{Bi} = 0.14$. The tilt angle $\phi_m \simeq 57^\circ$.

2. For the "intermediate" beams with $V_b/V_A = 10$, $n_b/n_0 = 0.03$, $\bar{j}_b = 0.3$, and $V_{Tb}/V_A = 10$, the CCOI growth rate is quite large, $\gamma_m/\omega_{Bi} \simeq 0.1$, and is attained at $\mu_{bm} = 1.35$, $k_{zm}V_A/\omega_{Bi} = 0.13$. The corresponding tilt angle $\phi_m \simeq 46^\circ$.

3. The "diffuse" beams propagate along magnetic fields linked to the regions where the shock is quasi-parallel (the angle between the shock normal and magnetic field $\mathbf{B}_0$ is less than 45°). Using the "representative" values for these beams, $n_b/n_0 = 0.03$, $V_b/V_A = 5$ (hence $\bar{j}_b = 0.15$), and $V_{Tb}/V_A = 15$, we find the CCOI growth rate $\gamma_m/\omega_{Bi} \simeq 0.04$. The characteristic wavenumbers of excited waves are $\mu_{bm} = 1.2$, $k_{zm}V_A/\omega_{Bi} = 0.06$, such that the angle between $\mathbf{k}_m$ and $\mathbf{B}_0$ is about $\phi_m \simeq 54^\circ$.

As is seen from the above estimations, the "intermediate" beams are most favorable for the CCOI. With larger beam currents and/or thermal velocities, the CCOI growth rate is larger and the tilt angle is smaller (see Figure 6 for specific

numbers). For example, for the "intermediate" beam with $V_b/V_A = 10$, $V_{Tb}/V_A = 10$, and elevated density $n_b/n_0 = 0.09$, the instability is very strong, $\gamma_m/\omega_{Bi} \simeq 0.4$, and the tilt angle $\phi_m \simeq 20^\circ$.

Oblique waves with ϕ_m scattered between 0° and 180° were observed by Cluster in the foreshock, with the dominant wave fraction concentrated in the range $\phi_m \simeq 10^\circ$–30° and several minor peaks (see Figure 13 by Narita et al. 2006). Two peaks at different ϕ_m were also observed by Hobara et al. (2007) for 30 s waves. In addition to the main peak, Narita et al. (2006) also found minor fractions of more oblique waves in the quasi-parallel foreshock: forward fraction at $\phi_m \simeq 40^\circ$–70°, backward fractions at $\phi_m \sim 140^\circ$, and $\phi_m \sim 170^\circ$. In the quasi-perpendicular foreshock, the sub-dominant wave fractions at $\phi_m \sim 60^\circ$ and $\phi_m \lesssim 90^\circ$ are relatively larger than in the quasi-parallel foreshock. The wave-mode composition of these spectra, especially in the quasi-perpendicular foreshock (see Narita et al. 2006), is uncertain. Multiple spectral peaks and variable properties of observed waves suggest that several modes and instabilities contribute to the foreshock wave spectra.

To generate the dominant wave fraction at $\phi_m \simeq 10^\circ$–30°, the CCOI needs a large enough $\bar{j}_b$ and/or V_{Tb}/V_A from the range above the red line corresponding to 30° in Figure 6. Less restrictive conditions are required for the generation of sub-dominant wave spectra in quasi-perpendicular foreshocks (values of $\bar{j}_b$ and V_{Tb}/V_A along the 60° line in Figure 6 for the peak at $\phi_m \sim 60^\circ$ and just above the dashed line for the very oblique waves at $\phi_m \lesssim 90^\circ$).

If we turn now to the full wavenumber distributions of observed waves (Figure 9 in Narita et al.), we find a quite different picture with two aboutequal peaks that do not map onto unequal peaks on the angle distributions shown in Figure 13 of Narita et al. The peak at $k_m\rho_i \sim 0.4$ in the quasi-perpendicular foreshock can be easily generated by the CCOI with relatively small values of $\bar{j}_b$ and V_{Tb}/V_A around the line $k_m\rho_b = k_m\rho_i\sqrt{T_b/T_i} \simeq 1.5$ in Figure 5. Another peak in the quasi-perpendicular foreshock at smaller $k_m\rho_i \approx 0.06$ is more difficult to reproduce by the CCOI, which would require quite high values of $T_b/T_i > 10^2$ more typical for the quasi-parallel foreshock. In the quasi-parallel foreshock, both peaks can be generated by the CCOI under reasonable beam and plasma conditions.

There is an apparent contradiction between CCOI properties and properties of foreshock waves observed by Narita et al. (2006). Namely, Narita et al. estimated the real wave frequency in the plasma frame $\sim 0.2\omega_{Bi}$, which contradicts the aperiodic nature of perturbations generated by the CCOI. One should, however, note that in a non-stationary plasma with time-varying parameters, the wave frequency and polarization are not conserved quantities but evolve in time (see, e.g., Mendonça 2009; Lade et al. 2011 and references therein). Therefore, in the highly dynamic foreshock environment, the aperiodic waves generated by the CCOI can develop significant real frequencies and contribute to the wave spectra observed by Narita et al. (2006). For example, from Figure 3, it follows that the aperiodic waves generated by the CCOI when the current was $j_b = 0.4$ possess the parallel wavenumber $k_z V_A \approx 0.2\omega_{Bi}$, which, being conserved in time, increases the wave frequency to $\sim 0.1\omega_{Bi}$ when the time-varying $\bar{j}_b$ drops below 0.2 and to $\sim 0.2\omega_{Bi}$ when $\bar{j}_b$ drops below 0.1. The wave phase velocity also varies in the time-varying conditions, which makes the wave-mode identification based on the phase velocity histograms (Figures 10–12 in Narita et al. 2006) even more uncertain. Particular regimes of the wave temporal evolution have been studied insufficiently and further investigations are needed for this process in the foreshock conditions.

Since the stable range is bounded by the threshold current, $\bar{j}_b = \bar{j}_{thr}$, and the threshold current $\bar{j}_{thr}$ depends on V_{Tb}/V_A (Equation (12)), the measured values of $\bar{j}_b$ and V_{Tb}/V_A should be statistically constrained. Namely, if the boundary in the scatter plot of measured values ($\bar{j}_b$, V_{Tb}/V_A) can be approximated analytically as

$$\bar{j}_b \frac{V_{Tb}}{V_A} \simeq a_{CCOI}, \tag{23}$$

with $a_{CCOI} = 1.5$–2, that would suggest that the beam currents and/or temperature are regulated by the CCOI. We are not aware of such correlation measurements in terrestrial foreshocks.

The observed satellite-frame frequency is determined by the large Doppler shift and can be estimated as $\omega_{sat} \simeq k_\perp V_{sw}\sin\theta_{VB} \simeq \omega_{Bi}(V_{sw}/V_{Tb})\mu_{bm}\sin\theta_{VB}$, where θ_{VB} is the angle between the solar wind speed and $\mathbf{B}_0$. Keeping in mind that $\mu_{bMAX} = 0.9$–2, with the same "representative" values as above, and $\theta_{VB} \simeq \pi/4$, we obtain $\omega_{sat} \simeq (0.1$–$1)\omega_{Bi}$. The waves in this frequency range are regularly observed by satellites.

In the time intervals when $\theta_{VB} \simeq 0$, the satellite-frame frequencies of the CCOI fluctuations are determined by the (smaller) parallel wavenumbers and ω_{sat} reduces to $\sim 0.05\omega_{Bi}$. Consequently, we have another expected observational signature of the CCOI: the measured wave energy in the low-frequency band $(0.01$–$0.1)\omega_{Bi}$ should be larger in the cases $\theta_{VB} \simeq 0$ than in the cases $\theta_{VB} \gtrsim \pi/4$. We are not aware if such a trend is observed.

6. DISCUSSION

To understand the physical nature of the CCOI, we note that the destabilizing term proportional to $\bar{j}_b^2$ in the dispersion equation (Equation (9)) comes from the product of non-diagonal elements ε_{xy} and $\varepsilon_{yx} = -\varepsilon_{xy}$ of the dielectric tensor (Equation (5)), which are dominated by the background electron current j_e and the reduced beam current $A_0'(\mu_b^2)j_b$:

$$\varepsilon_{xy} = \varepsilon_{xy}^{(e)} + \varepsilon_{yx}^{(b)} \simeq i\left(\frac{4\pi}{B_0}\right)\left(\frac{k_z c}{\omega^2}\right)\left[n_0 e V_e + n_b e V_b A_0'\left(\mu_b^2\right)\right]$$
$$\simeq i\frac{\omega_{Pp}}{\omega}\frac{k_z c}{\omega}\left[1 + A_0'\left(\mu_b^2\right)\right]\bar{j}_b. \tag{24}$$

The zero net current condition $n_0 e V_e = n_b e V_b$ is used in the above expression.

From the electron contribution $\varepsilon_{xy}^{(e)}$, and the beam contribution $\varepsilon_{yx}^{(b)}$, we see that the fluctuating electron and beam ion currents can be expressed via the fluctuating magnetic field $\delta\mathbf{B}_\perp$ as $\delta\mathbf{j}_{e\perp} \simeq j_e\delta\mathbf{B}_\perp/B_0$ and $\delta\mathbf{j}_{b\perp} \simeq A_0'(\mu_b^2)j_b\delta\mathbf{B}_\perp/B_0$, respectively. These first-order currents have the following simple interpretation. The frozen-in electron current, flowing along the curved field lines, $\mathbf{B} = \mathbf{B}_0 + \delta\mathbf{B}_\perp$, deviates in the $\delta\mathbf{B}_\perp$ direction and thus develops a perpendicular component $\delta j_{e\perp}/j_e = \delta B_\perp/B_0$. On the other hand, the ion-beam current is partially unfrozen by the large gyroradius of the beam ions, which reduces $\delta j_{b\perp}$ by a factor $A_0'(\mu_b^2)$. As a result, even if the zero-order currents j_e and j_b are compensated ($j_b + j_e = 0$), they induce the first-order electron and beam ion currents that are not compensated, $\delta\mathbf{j}_{e\perp} + \delta\mathbf{j}_{b\perp} \neq 0$. The resulting first-order net current $\delta\mathbf{j}_\perp \simeq (1 + A_0'(\mu_b^2))j_b\delta\mathbf{B}_\perp/B_0$ makes Alfvén waves aperiodically unstable. The CCOI is therefore the current-driven instability in

two respects: (1) the instability source is the compensated zero-order currents, which generate (2) the uncompensated first-order current $\delta j_\perp$ responsible for the instability.

As follows from the above explanation, the physical nature of the CCOI is different from that of the FHIs, including parallel and oblique fire hoses driven by the effective anisotropic plasma pressure $T_\parallel > T_\perp$ (see, e.g., Hellinger & Matsumoto 2000).

Given its non-resonant driving mechanism, the CCOI depends on the bulk parameters of plasma species rather than on the local behavior of their velocity distributions. By using other velocity distributions instead of a Maxwellian one, we would obtain similar results with the destabilizing factor proportional to j_b, but with another demagnetization function replacing $A_0'(\mu_b^2)$. The behavior of any particular demagnetization function is expected to be as regular as $A_0'(\mu_b^2)$, with the same limits $\to -1$ at $k_\perp \to 0$ and $\to 0$ at $k_\perp \to \infty$. The instability is therefore expected to be quite robust and, contrary to the resonant current-driven instabilities, does not suffer from the fast saturation by the local plateau formation in the particle velocity distributions.

It is interesting to note that the growth rate of the Winske–Leroy instability in the well-over-threshold regime (their Equation (16)) can be expressed in terms of the beam current as $\gamma_{\rm WL} \simeq 0.5\bar{j}_b\omega_{Bi}$, which is exactly the same scaling as for the CCOI (Equation (19)). The same scaling suggests that both instabilities are driven by the same factor. Winske & Leroy (1984) have stressed that their strong non-resonant instability is not of the fire-hose type, but did not explain its physical nature. After inspecting derivations by Winske & Leroy (1984), we found that their most unstable regime (Equations (14)–(16) in their paper) is indeed driven by the same factor as the CCOI: the non-compensated wave currents developed in response to the compensated global currents.

A similar compensated-current instability of MHD-like modes has been found recently by Bell (2004, 2005). The Bell instability arises in response to the currents induced by cosmic rays around supernova remnants. Again, using Equation (5) of Bell (2005), it is easy to see that this instability has a maximum $\gamma_{\rm Bell} \simeq 0.5\bar{j}_b\omega_{Bi}$ attained at $|k_{z\rm m}|V_A/\omega_{Bi} = 0.5\bar{j}_b$. These expressions are exactly the same as for the Winske–Leroy instability. Also, similarly to the Winske–Leroy instability, the Bell instability maximizes at parallel propagation, $k_\perp = 0$. Bell's analysis differs from Winske & Leroy's analysis in how the background plasma, beam, and unstable modes are treated. Winske & Leroy (1984) used a fully kinetic theory assuming a shifted Maxwellian proton beam, whereas Bell (2004) reduced the problem to the "hybrid" MHD-kinetic one (MHD with the currents calculated kinetically) and used a power-law momentum distribution of the beam ions.

Both the Winske–Leroy and the Bell instabilities arise because of essentially the same physical effect: suppression of the wave response to the beam ion current by the large factor $k_z V_{bz}/\omega_{Bi} > 1$ (the parallel dispersion effect). The wave response to the background electron-current survives such suppression because the electrons with small $k_z V_{ez}/\omega_{Be} < 1$ remain magnetized. This implies a physical interpretation somehow different from that proposed by Bell (2004, 2005), who described it in terms of a large ion gyroradius (a *perpendicular* ion scale). In our opinion, the reducing factor in this case is the large *parallel* scale of the beam ions, $\lambda_{bz} = V_{bz}/\omega_{Bi}$, which defines the ion-cyclotron time-of-flight distance along the background magnetic field. If the *parallel* wavelength is comparable to or shorter than this distance, $k_z\lambda_{bz} > 1$, the wave response to the beam current is reduced by the effective ion demagnetization. Both the Winske–Leroy and Bell instabilities are strongest at parallel propagation and are physically the same instability that can be called the compensated-current parallel instability (CCPI).

The effects of the large ion gyroradius in the beam, which are determined by the *perpendicular* ion motion and *perpendicular* wavenumber dispersion (factor $k_\perp\rho_{b\perp} = k_\perp V_{Tb\perp}/\omega_{Bi}$), are considered in the present paper. Similarly to CCPI, the wave response to the beam ion current is also suppressed in the CCOI, but the nature of this suppression is different. Contrary to CCPI, for which the parallel dispersive effects of finite $k_z\lambda_{bz}$ are important, the CCOI is caused by the perpendicular dispersive effect of finite $k_\perp\rho_{b\perp}$. Consequently, the CCOI develops in a quite different wavenumber range characterized by large $k_\perp$.

Concluding the above comparisons, we expect several peaks in the spectrum of unstable fluctuations in the compensated-current systems with ion beams. In particular, two current-driven instabilities arise in the case of hot and fast ion beams: one at parallel propagation $\phi = 0$ (i.e., at $k_\perp = 0$) for CCPI studied by Winske & Leroy (1984) and Bell (2004) and another at $\phi = \phi_{\rm m}$ defined by Equation (21) (i.e., at $k_\perp = k_{\perp\rm m}$) for the CCOI studied here. Because of the same destabilizing factor $\bar{j}_b$, CCPI and the CCOI have the same asymptotic scaling $\gamma_{\rm CCPI} \sim \gamma_{\rm CCOI} \sim 0.5\bar{j}_b\omega_{Bi}$ at large $\bar{j}_b \gg \bar{j}_{\rm thr}$. However, in the cases where $\bar{j}_b$ is not much larger than $\bar{j}_{\rm thr}$, the additional degree of freedom $k_\perp\rho_{b\perp} \neq 0$ makes the CCOI more flexible in finding larger growth rates as compared with the CCPI.

For hot and fast ion beams ($V_{Tb} \geqslant V_b \gg V_A$), the ion two-stream and Buneman instabilities are inefficient and the main competitors of the CCOI are the left- and right-handed polarized resonant instabilities discussed above (Gary 1985) and the non-resonant instabilities studied by Sentmann et al. (1981), Winske & Leroy (1984), and Bell (2004). For example, from the upper curve in Figure 3(b) by Gary (1985) for the left-handed polarized instability driven by the beam $n_b/n_0 = 0.02$ and $V_b/V_A = 10$, we find a growth rate $\gamma_{\rm LH}/\omega_{Bi} \simeq 0.07$. For the same plasma parameters, the CCOI growth rate is somewhat larger, $\gamma_{\rm m}/\omega_{Bi} \simeq 0.08$. This value is also larger than that for the Winske–Leroy non-resonant instability at the same parameters. Since the differences are not large, all these instabilities can compete in typical foreshock conditions.

At lower beam velocities, $V_A \leqslant V_b \leqslant 2V_A$, and lower beam temperatures, $T_b \sim T_p$, resonant instabilities of the parallel fast and oblique Alfvén modes are stronger than the parallel ones (Voitenko 1998; Daughton et al. 1999; Gary et al. 2000; Voitenko & Goossens 2003; Verscharen & Chandran 2013) and can compete with the CCOI. Since the CCOI theory for this parameter range is not yet developed, a quantitative comparison of the CCOI with these instabilities is postponed to a future study.

7. CONCLUSIONS

We found a new oblique Alfvénic instability, the CCOI, driven by compensated currents flowing along the mean magnetic field. The instability arises on the Alfvén mode dispersion branch due to the coupling to the fast mode via the current term proportional to $\bar{j}_b$. The instability is enforced by the increasing current $\bar{j}_b$ and beam thermal spread V_{Tb}.

The physical mechanism of this instability is as follows. Because of the finite ion gyroradius effects, the oblique Alfvénic perturbations react differently on the current carried by the beam ions and the current carried by the electrons. Namely, the wave response to the beam ion current is reduced by averaging over

the large ion gyroradius, whereas the small electron gyroradius leaves the electron-current response practically unaffected. Ultimately, the difference between the electron and ion responses results in a net first-order current that shifts the Alfvén wave frequency squared below zero, making the wave aperiodically unstable.

Our results show that in many astrophysical and space plasma settings comprising ion beams and return electron currents, the CCOI is a strong competitor for the CCPIs studied by Winske & Leroy (1984) and Bell (2004, 2005), as well as for the beam-driven fire hose and kinetic instabilities.

The main CCOI properties are as follows.

1. The instability is driven by the perpendicular dispersive effects of finite $k_\perp \rho_{b\perp}$, which result in the uncompensated wave currents developed in response to the compensated zero-order currents.

2. The threshold beam current is $\bar{j}_{\rm thr} \simeq 1.33 V_A/V_{Tb}$ and the instability growth rate (maximal increment) is

$$\begin{cases} \gamma_{\rm m} \simeq 0.67(\bar{j}_b - \bar{j}_{\rm thr})\omega_{Bi}, & \text{for} \quad \bar{j}_{\rm thr} < \bar{j}_b < 2\bar{j}_{\rm thr}, \\ \gamma_{\rm m} \simeq 0.5\,\bar{j}_b \omega_{Bi}, & \text{for} \quad 2\bar{j}_{\rm thr} \leqslant \bar{j}_b < 2. \end{cases} \tag{25}$$

The upper bound on $\bar{j}_b$ appears here because of our initial approximations, which restrict the range of tractable beam currents to $\bar{j}_b < 2$ (this follows from the low-frequency approximation used, $\gamma_{\rm m}^2 < \omega_{Bi}^2$).

3. The approximate expressions (Equation (25)) are valid in the range $1.33 V_A/V_{Tb} < \bar{j}_b < 2$, which is not empty if the beam temperature is sufficiently high to make $V_{Tb}/V_A > 0.7$. The $k_\perp$-dependent growth rate γ_μ (Equation (16)) is valid for stronger currents $\bar{j}_b > 2$, but only in the wavenumber ranges where $\gamma_\mu < \omega_{Bi}$.

4. The range of unstable perpendicular wavenumbers is narrow in the near-threshold regime, but expands as the beam current grows. Consequently, a wide-band wave spectrum can be generated well above the threshold.

5. We found that the optimal perpendicular wavenumber for the instability is $k_\perp \rho_b \gtrsim 1$ and that the instability is very strong, $\gamma_{\rm m} \simeq (0.1\text{–}0.5)\omega_{Bi}$ for reasonable beam currents $\bar{j}_b \simeq 0.1\text{–}1$.

6. An essential characteristic of the fluctuations generated by the CCOI is their obliquity. In the near-threshold regime $\bar{j}_{\rm thr} < \bar{j}_b < 2\bar{j}_{\rm thr}$, the generated fluctuations are very oblique, $50^\circ < \phi_{\rm m} < 90^\circ$. Well above the threshold, the instability becomes less oblique and $\phi_{\rm m}$ can drop below 20° for strong enough beam currents.

Such oblique fluctuations, regularly measured in terrestrial foreshocks, can be explained by the CCOI. Other competing instabilities, like the left-/right-handed resonant (Gary 1985), fire-hose (Sentmann et al. 1981), "anti-parallel non-resonant" (Winske & Leroy 1984), and "parallel non-resonant" (Bell 2004, 2005) instabilities are magnetic field-aligned, and hence cannot explain the oblique fluctuations.

This research was supported by the Belgian Science Policy Office (through Prodex/Cluster PEA 90316 and IAP Programme project P7/08 CHARM) and by the European Commission (through FP7 Program project 313038 STORM). We thank the referee for useful comments and suggestions that helped us to improve this paper.

REFERENCES

Alexandrov, A. F., Bogdankevič, L. S., & Rukhadze, A. A. 1984, Principles of Plasma Electrodynamics (Berlin: Springer)
Bell, A. 2004, MNRAS, 353, 550
Bell, A. 2005, MNRAS, 358, 181
Büchner, J., & Elkina, N. 2006, PhPl, 13, 082304
Chen, L., & Wu, D. J. 2012, ApJ, 754, 123
Daughton, W., Gary, S. P., & Winske, D. 1999, JGR, 104, 4657
Duijveman, A., Hoyng, P., & Ionson, J. A. 1981, ApJ, 245, 721
Gary, S. P. 1985, ApJ, 288, 342
Gary, S. P., Yin, L., Winske, D., & Reisenfeld, D. B. 2000, GeoRL, 27, 1355
Hellinger, P., & Matsumoto, H. 2000, JGR, 105, 10519
Hobara, Y., Walker, S. N., Balikhin, M., et al. 2007, JGR, 112, A07202
Lade, R. K., Lee, J. H., & Kalluri, D. K. 2011, J. Infrared Milli. Terahz. Waves, 32, 960
Malovichko, P. P. 2007, KPCB, 23, 185
Malovichko, P. P., & Iukhimuk, A. K. 1992a, Ge&Ae, 32, 163 (in Russian)
Malovichko, P. P., & Iukhimuk, A. K. 1992b, KFNT, 8, 20 (in Russian)
Marsch, E. 2006, LRSP, 3, 1 (http://solarphysics.livingreviews.org/Articles/lrsp-2006-1/)
Mendonça, J. T. 2009, NJPh, 11, 013029
Narita, Y., Glassmeier, K.-H., Forna çon, K.-H., et al. 2006, JGR, 111, A01203
Paschmann, G., Sckopke, N., Papamastorakis, I., et al. 1981, JGR, 86, 4355
Sentmann, D., Edmiston, J. P., & Frank, L. A. 1981, JGR, 86, 2039
Singh, K. A. P., & Subramanian, P. 2007, SoPh, 243, 163
Tsurutani, B., & Rodriguez, P. 1981, JGR, 86, 4317
Voitenko, Iu. M., Likhachev, A. A., & Iukhimuk, A. K. 1980, GeoZh, 2, 76 (in Russian)
Voitenko, Y. 1995, SoPh, 161, 197
Voitenko, Y. 1998, SoPh, 182, 411
Voitenko, Y., & Goossens, M. 2003, SSRv, 107, 387
Verscharen, D., & Chandran, B. D. G. 2013, ApJ, 764, 88
Winske, D., & Leroy, M. M. 1984, JGR, 89, 2673